Modeling of an automotive exhaust gas converter at low temperature aiming at control application

1999-01-3623

Modeling of an Automotive Exhaust Gas Converter at Low Temperatures Aiming at Control Application

M. Balenovic, J. H. B. J. Hoebink and A. C. P. M. Backx
Eindhoven University of Technology

A. J. L. Nievergeld
Aspen Tech Europe

ABSTRACT

The LEV/ULEV emission standards pose challenging problems on automotive exhaust gas treatment. This increases the need for good catalytic converter models, which can be applied for control. A dynamic converter model was made on the basis of first principles, accounting for the accumulation of mass in the bulk gas phase, in pores of the washcoat and on the catalytic surface, as well as for the energy accumulation in the gas and solid phase. The basis for the model is the elementary step kinetics of the individual global reactions. The main purpose of the model is to describe the low temperature behavior of the converter, when the majority of the emissions occur. The light-off process is analyzed in detail with different inputs. The biggest improvement occurs when secondary air is injected in front of the converter. The converter model is also coupled with a simple SI engine model to investigate the dynamic behavior of the whole system.

INTRODUCTION

To meet the more stringent emission standards car and catalyst manufacturers put a lot of effort in reduction of harmful exhaust substances such as CO, HC and NOx. This can be done by reducing the engine out emissions and/or increasing the efficiency of the exhaust gas aftertreatment, i.e. the catalytic converter. The 3-way catalytic converter proves to be a good solution for the exhaust gas aftertreatment being able to simultaneously convert CO, HC and NOx. To achieve the highest conversion the converter has to be operated close to stoichiometry and the converter temperature has to be high enough. The first problem leads to the development of engine air-fuel ratio control strategies [1,2,3]. The problem of converter temperature leads to high emissions during the cold start phase, which attributes to 70-80% of all harmful substances emitted during the FTP or EURO test cycles. Electrical heating of the monolith converters and/or secondary air injection can be used to speed up catalyst light-off and reduce the cold start emissions [4,5,6,7].

The catalytic converter behavior under different operating conditions can be investigated experimentally [8,9,10], and by means of modeling. The computer models are very beneficial for the converter optimization. They can be used to optimize physical properties of the converters (geometry, washcoat formulation etc.) as well as to describe the converter's static and dynamic behavior, which can lead, to new control strategies. Typical models are based on one dimensional conversion, heat and mass transfer modeling [11,12,13,14]. These models normally comprise steady state reaction kinetics, with lumped surface adsorption-desorption phenomena, and dynamic behavior of oxygen storage and release by ceria. Models on the same basis can be implemented for simulation of heated monolithic converters [6].

The converter model in a simplified form can be directly used for control purposes. One reported application uses an oxygen storage model in an adaptive control scheme to keep the level of stored oxygen within the catalyst oxygen storage capacity [15].

A fully transient converter model using elementary step kinetics was developed in this study mainly to investigate the catalyst behavior at low temperatures. Such a model gives a better insight into processes taking place during catalyst warm-up, but leads to higher numerical complexity. The further intention is to use this model to obtain optimal control strategies for emission reduction and to apply them in model-based control schemes. The model in this stage is quite complicated, and should be simplified in the future by identification techniques to be directly used for control.

MODEL DESCRIPTION

The 3-way catalytic converter model is based on a one-dimensional adiabatic reactor model and elementary step kinetics from the literature. Carbon monoxide, nitric oxide, ethene, ethyne and oxygen are the exhaust components taken into consideration.

REACTOR MODEL – The one dimensional adiabatic reactor model is based on the models reported by Lie et al. [16] and Nievergeld et al. [17]. To simplify the model with regard to computational efforts, some assumptions have been made. The most important ones are mentioned here. The radial gas velocity distribution is assumed to be uniform. In practice the flow velocity in the outer channels might be lower than in the inner channels due to a short divergent inlet of the monolith. The reactor operates adiabatically, thus the ambient heat losses are not considered. The walls of the ceramic channels are assumed to be impenetrable to gas and all channels have equal diameters. Under these conditions only one channel can be modeled as representative for the whole monolith. Only axial concentration and temperature gradients in the gas phase are considered. Mass and heat transfer from bulk gas to washcoat are described by constant heat and mass transfer coefficients, based on the limit values of the Nusselt and Sherwood numbers for laminar flow. The laminar flow in the small diameter channels is approached as plug flow since the Taylor criterion [18] is obeyed.

The model consists of a set of continuity equations for the reactants in the bulk gas phase, in the pores of the washcoat and on the catalyst surface, as well as energy equations in the bulk gas and solid phase. The continuity equations for reactant i (i=CO,O_2,NO,C_2H_2,C_2H_4) in the bulk gas phase are given by:

$$\varepsilon\rho_f \frac{\partial}{\partial t}\left(\frac{C_{f,i}}{\rho_f}\right) = -\Phi_m^{\sup}\frac{\partial}{\partial x}\left(\frac{C_{f,i}}{\rho_f}\right) - \rho_f k_{f,i} a_v \left(\frac{C_{f,i}}{\rho_f} - \frac{C_{s,i}}{\rho_f}\right) \quad (1)$$

and in the solid phase by:

$$\varepsilon_w\rho_f \frac{4\varepsilon d_w}{d_b}\frac{\partial}{\partial t}\left(\frac{C_{s,i}}{\rho_f}\right) = \rho_f k_{f,i} a_v \left(\frac{C_{f,i}}{\rho_f} - \frac{C_{s,i}}{\rho_f}\right) - a_{cat}(r_{a,i} - r_{d,i}) \quad (2)$$

The last term in eq. (2) accounts for the adsorption and desorption of species to and from the noble metal and oxygen storage surface. The continuity equations for the surface species will be explained in the next subsection. The dependent variables are expressed as C/ρ_f to correct for the density changes as a function of the axial coordinate due to non-uniform temperatures. The energy equations in the gas and solid phase are given by:

$$\varepsilon\rho_f c_{pf}\frac{\partial T_f}{\partial t} = -\Phi_m^{\sup} c_{pf}\frac{\partial T_f}{\partial x} - \alpha a_v (T_f - T_s) \quad (3)$$

$$(1-\varepsilon)\rho_s c_{ps}\frac{\partial T_s}{\partial t} = \lambda_s (1-\varepsilon)\frac{\partial^2 T_s}{\partial x^2} + \alpha a_v (T_f - T_s) + a_{cat}\sum_j \left(-\Delta_r H\right)_j r_j \quad (4)$$

The reaction heat generation is accounted for in the last term of equation (4). It is calculated using the rates of the global reactions, r_j. This is allowed since the heat capacity of the reactor is much higher then the heat production due to changing surface coverages [19].

KINETIC MODEL – Typical hydrocarbons used in exhaust gas converter modeling are propane and propene. It is disputable whether these components should be considered as typical for hydrocarbons. They are not present in exhaust gas in large amounts [20]. In the current work ethene and ethyne were taken as hydrocarbons. The former concerns 25 mol% of the hydrocarbons [20], while the latter accounts for 20 mol% and moreover has been shown to inhibit the oxidation of both CO and other hydrocarbons notably at low temperatures [21], as often met in a cold engine start. The elementary steps of the kinetic model are as follows:

$$\begin{aligned}
1 \quad & CO + * \leftrightarrow CO* \\
2 \quad & O_2 + 2* \rightarrow 2O* \\
3 \quad & CO + O* \rightarrow OCO* \\
4 \quad & NO + * \leftrightarrow NO* \\
5 \quad & C_2H_4 + 2* \leftrightarrow C_2H_4** \\
6 \quad & C_2H_2 + 4* \leftrightarrow C_2H_2**** \\
7 \quad & NO* + * \rightarrow N* + O* \\
8 \quad & CO* + O* \rightarrow CO_2 + 2* \\
9 \quad & OCO* \rightarrow CO_2 + * \\
10 \quad & NO* + N* \rightarrow N_2 + O* + * \\
11 \quad & 2N* \rightarrow N_2 + 2* \\
12 \quad & C_2H_4** + 4O* \rightarrow 2CO* + 2H_2O + 4* \\
13 \quad & C_2H_2**** + 5O* \rightarrow 2CO_2 + H_2O + 9* \\
14 \quad & O_2 + 2s \rightarrow 2Os \\
15 \quad & CO* + Os \rightarrow CO_2 + * + s
\end{aligned} \quad (5)$$

The '*' in the above elementary steps denotes the noble metal site, while 's' denotes the ceria surface site, thus including the oxygen storage capacity of the catalyst into the model. Since an elementary step kinetic model for a realistic exhaust gas and one catalyst is presently not available in the literature, the above mentioned steps and their corresponding kinetic parameters were taken from several sources as the major goal of this research was to investigate the interaction and competition of individual global reactions. Such an approach has been shown useful in understanding converter behavior [17, 22]. The steps involving CO and NO were taken from Oh et al. [23]. Ethene and ethyne oxidation was based on the work of Sant et al.[24]. They proposed two models for ethene oxidation: a model for low oxygen concentration and a model for high oxygen concentration. The ethene oxidation used in this study is based on the low oxygen concentration model since ethene normally reacts after CO and ethyne have been oxidized, thus at low oxygen concentration levels. On the other hand, ethyne is first to be oxidized and therefore oxygen rich conditions can be assumed. Since there is no elementary step kinetic

model for ethyne oxidation available in the literature, the model from Sant et al. for high oxygen concentration has been adapted to describe the experimental data from Mabilon et al. [21]. The kinetic data for reaction of CO and oxygen stored on the ceria surface were taken from Nibbelke et al. [25]. The diffusion of oxygen from the bulk to the surface of ceria and viceversa is not considered here because it becomes an important process only at higher temperatures [25]. The possibility of CO adsorption on a catalytic site already occupied by oxygen, leading to OCO* formation, was also included in the model [25]. This effect was observed when a CO stream was imposed on an oxygen covered catalyst surface.

The adsorption rate of component i (i=CO, O_2, NO, C_2H_2 and C_2H_4) on the noble metal site is given by:

$$r_{a,i} = k_{a,i} L_{NM} C_i \theta_* \tag{6}$$

while the adsorption rate coefficients are obtained from the kinetic gas theory:

$$k_{a,i} = \frac{1}{L_{NM}} \sqrt{\frac{RT}{2\pi M_i}} s_i^0 \tag{7}$$

The desorption rate of adsorbed species j (j=CO*, NO*, C_2H_4** and C_2H_2****) is proportional to the surface coverage of that species and is given by:

$$r_{d,j} = k_{d,j} L_{NM} \theta_j \tag{8}$$

Oxygen desorption can be neglected at the temperatures considered. The rates of surface reactions are proportional to the product of surface coverages of involved species (x,y):

$$r_r = k_r L_{NM} \theta_x \theta_y \tag{9}$$

Both desorption and surface reaction rate coefficients are of the Arrhenius type:

$$k_{r,d} = A_{r,d} \exp\left(-\frac{E_{act\,r,d}}{RT}\right) \tag{10}$$

Basically the same rate equations, as described above, are applied for the adsorption of oxygen on the ceria surface and the reaction between oxygen and CO adsorbed on the noble metal surface. The only difference is that the oxygen storage capacity, L_{OSC}, is used instead of the noble metal capacity, L_{NM}.

Now the continuity equation for the species j adsorbed on the noble metal sites or oxygen storage surface can be written as follows:

$$L_{CAP} \frac{\partial \theta_j}{\partial t} = r_{a,j} - r_{d,j} + \sum_k r_{k,j} \tag{11}$$

where k denotes a certain surface reaction which involves the species j. L_{CAP} stands for either L_{OSC} or L_{NM}. Hence, the noble metal (oxygen storage) surface coverage of some species might change by adsorption from the gas phase, desorption from the catalyst surface or reaction on the catalyst surface.

NUMERICAL PROCEDURE – The model variables are concentrations of species in the gas phase and in the pores of the washcoat, catalyst surface coverages and temperatures in gas and solid phase, along the reactor axis. This leads to a system of nonlinear, partial differential equations (PDE) to be solved, which is quite a complex task. Therefore, the method of lines with the discretization in the axial direction was applied to transform the system into a larger set of ordinary differential equations (ODE), which is then solved using Backward Differentiation formulae (BDF) with variable order and variable size [26].

SIMULATION RESULTS AND DISCUSSION

Parameters indicating size and type of the converter are given in table 1.The inputs to the reactor are volumetric concentrations of the considered exhaust gas species, exhaust gas temperature and mass flow. The inlet concentrations are calculated as nonlinear functions of the normalized air/fuel ratio (A/F), λ. Inlet concentrations for air/fuel ratios used in simulations are given in table 2. The hydrocarbon fraction of ethyne, in most of the simulations, was set to 30%. The exhaust mass flow was kept constant at a typical value of 20g/s.

Table 1. Parameter values used in the reactor model

Reactor length	0.15	$m_{reactor}$
Converter void factor (ε)	0.6	-
Reactor cross-sectional area	$6\ 10^{-3}$	$m^2_{reactor}$
Channel diameter (d_b)	10^{-3}	m
Washcoat thickness (d_w)	$2.5\ 10^{-5}$	m
Washcoat surface area (a_{cat})	$1.24\ 10^4$	$m^2_{cat}\ m^{-3}_{reactor}$
Noble metal capacity (L_{NM})	$2.7\ 10^{-5}$	mol m^{-2}_{cat}
Oxygen storage capacity (L_{OSC})	$1.08\ 10^{-4}$	mol m^{-2}_{cat}

Table 2. Inlet concentrations used in simulations

λ	0.97	1	1.03
CO [vol %]	1.07	0.6	0.33
O_2 [vol %]	0.28	0.53	0.89
NO [ppm]	950	1200	1440
C_2H_4 [ppm]	795	700	655
C_2H_2 [ppm]	341	300	281
CO_2 [vol %]	12	12	12
H_2O [vol %]	10	10	10

STEADY STATE – Steady state conversion with respect to the feed temperature, for the stoichiometric A/F, is shown in fig. 1. Note that conversions at all temperatures have been calculated in steady state, and that is not the condition during the normal light-off of the reactor. It is clear that the species are converted in a sequence. First ethyne is converted, then CO, while NO and ethene need higher temperature for the conversion. In a case without the ceria oxygen storage capacity, CO conversion would be even more retarded because the presence of ethyne inhibits the CO adsorption on the catalyst surface. Existence of another path for the CO oxidation, via the oxygen stored on ceria, improves the CO light-off. Ethyne needs higher temperatures to be oxidized then CO or ethene but the adsorption rate of ethyne is, however, higher than the adsorption rate of other species. Therefore, ethyne occupies most of the noble metal surface at low temperatures, not permitting the other species to be converted. After ethyne is converted, CO conversion completes, which frees the catalytic surface for ethene and NO to be converted. Ethene has a low adsorption rate, but is easily oxidized with a help of the subsequent reaction between the intermediate product, adsorbed CO, and oxygen from ceria. NO is the last component to be converted as the recombination of N adatoms proceeds mainly at high temperatures. Steady state gas concentrations and catalyst surface coverages of the species along the reactor axis at the feed temperature of 480K are shown in figs. 2 and 3. The conversion along the reactor axis takes place in the same sequence as in fig. 1. CO conversion starts after ethyne is almost completely converted. NO and ethene conversions start when the majority of CO is converted. This sequence can be explained by analyzing the surface coverages along the reactor axis. In the first part of the reactor ethyne, NO and CO compete for the active sites. There is also little NO dissociation since the surface is fully covered. After all ethyne and CO have been converted, vacant sites become available for the adsorption of ethene and for more adsorption and subsequent dissociation of NO. Ethene surface coverage is very low throughout the whole reactor because it is easily oxidized by oxygen adsorbed on the surface. The oxygen surface coverage increases toward the end of the reactor because of gradually decreasing oxygen consumption by ethene. In the second part of the reactor the catalyst surface is mainly covered by nitrogen. This happens because NO relatively easily adsorbs on the surface, especially after ethyne and CO have been converted, and dissociates to oxygen and nitrogen adatoms. The process of N_2 formation (especially through the recombination of two N* adatoms) is, however, quite slow and leads to the increased nitrogen surface coverage. Fig. 3 also shows which fraction of the oxygen storage capacity is occupied along the reactor axis. Since the oxygen stored on the ceria surface reacts with CO on the noble metal in the first part of the reactor, less then 50% of the capacity is occupied. As the CO concentration decreases along the reactor axis, ceria becomes almost completely covered with oxygen.

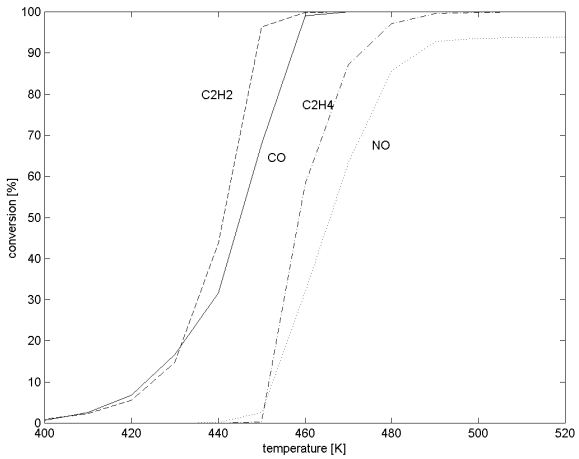

Figure 1. Steady state conversion versus feed temperature, with λ=1.

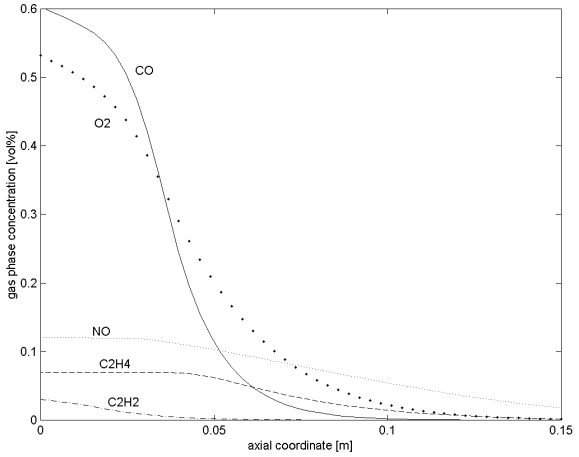

Figure 2. Gas phase concentration versus axial coordinate at a feed temperature of 480K, λ=1

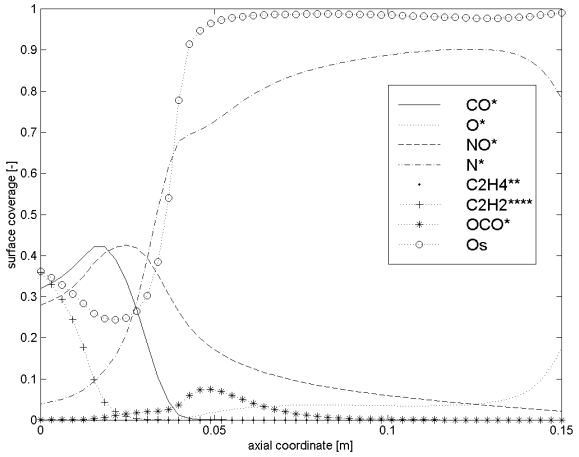

Figure 3. Noble metal and oxygen storage surface coverage versus axial coordinate at a feed temperature of 480K, λ=1.

INLET TEMPERATURE STEP RESPONSES – A step increase in the feed temperature from 400 to 500K causes reactor light-off. Fig. 4 shows the conversion of the species after the step has been imposed. There are two cases: the first is under the normal conditions, λ=1, while in the second case the ethyne amount was diminished to 10% of hydrocarbons. The light-off sequence is again the same as in the previous cases. In the second case the inlet ethyne concentration is lower, which reduces the ethyne-based inhibition and improves the light-off of all other species. Thus, it has been shown again that the inhibition process is inherently included in the model via the elementary steps. Note that the steady state conversion of NO and ethene have been increased and decreased respectively in the second case. This is the result of the changed hydrocarbon composition, which has slightly changed the input λ to rich, although the total molar concentration of hydrocarbons has not been changed.

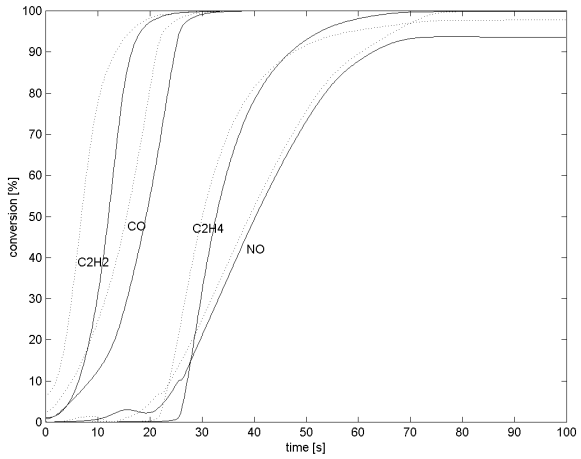

Figure 4. Conversions after a step increase of the feed temperature from 400 to 500K. Solid lines – ethyne forms 30% of hydrocarbons; dashed lines – ethyne forms 10% of hydrocarbons.

DYNAMIC BEHAVIOR OF THE CONVERTER – During normal operation of the converter it almost always operates in the dynamical regime. The typical engine control system produces oscillations of the inlet concentrations to the converter. These oscillations typically have amplitudes of 2-3% (expressed in λ) around the stoichiometry, and a frequency around 1Hz.

Converter dynamic behavior has been investigated by applying step changes of the converter input λ value between lean, λ=1.02 and rich, λ=0.98. Fig. 5 shows calculated λ responses at the converter outlet. Output lambda value is shown here because it is a measurable value in a typical exhaust control system. By definition, the lambda value does not change in the steady state. It is obvious that the main dynamic behavior of the converter is imposed through the oxygen storage and release on ceria. Step responses are very fast without the oxygen storage capacity of the converter. This shows that the change between two steady states on the noble metal surface occurs almost instantly at the given time scale. When the oxygen storage is included the responses are clearly slower. Oxygen stored at the ceria surface reacts with CO adsorbed on the noble metal surface after the lean-rich step. When the corresponding rate coefficient is increased this reaction becomes faster and more CO can react with the stored oxygen in the beginning. This leads to higher lambda values in the beginning of the transient, while the steady state is also reached faster. During the rich-lean step the most important coefficient is the rate of oxygen adsorption on the ceria. The rate of CO oxidation does not influence this transient. The oxygen storage capacity, as expected, is a very important parameter too. A higher OSC leads to slower lambda responses, because either there is more oxygen to react with CO, or it takes more time to fill the available ceria surface. Hence, these parameters determine the dynamic behavior of the converter around stoichiometry, and are the most important to be considered in control strategies. Note that the modeled oxygen storage submodel includes only the oxygen stored at the ceria surface. Diffusion of oxygen from the bulk of ceria to the surface or vice versa is not included, but this process becomes more important at higher temperatures and leads to a large increase of the relevant oxygen storage capacity.

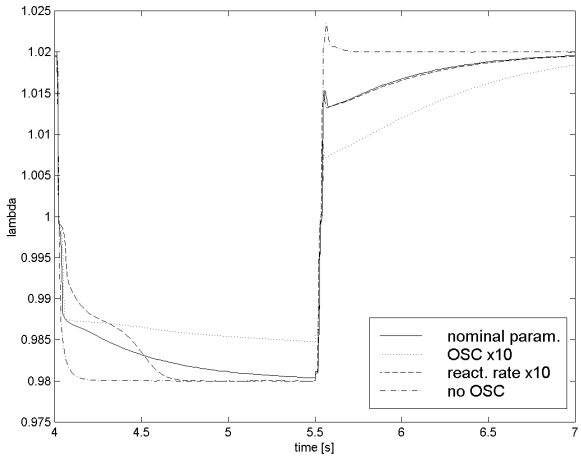

Figure 5. Converter outlet lambda responses on step changes of inlet lambda with different parameters relevant for the oxygen storage on ceria. The feed temperature is 480K.

COLD START STRATEGIES – Since the vast majority of the emissions occurs at low temperatures, during cold start of the engine, optimal converter warming-up strategies have to be considered. External heating of the converter and/or secondary air injection are standard additional measures for cold start. External heating has not been considered in this study, while secondary air injection will be discussed later. Many researchers have reported a conversion improvement due to oscillatory feed to the converter, which is the result of the control loop [8,10]. These reports have usually been based on

experimental work. Since this conversion improvement has been explained as the effect of nonlinear kinetics, one of the goals of this research was to examine the converter model behavior with oscillating input feeds. Detailed results can be found in [17]. The main conclusion of this research is that cyclic feeding can be beneficial only at temperatures below the light-off. Since the light-off temperatures are different for the individual reactants, the beneficial effects do not coincide at any temperature.

Increasing the inlet reactor temperature from 300K to 600K linearly over a time interval of 100s performed a typical cold start simulation. Four different inlet mixtures were applied to the converter: lean (λ=1.03), rich (λ=0.97), stoichiometric and oscillatory (A=0.02, f=1Hz). Oscillatory feed assumes sinusoidal oscillations of the input λ yielding nonlinear oscillations of CO, NO and HC. Fig. 6 presents conversions versus time for each individual reactant in all four cases. The conversion for the oscillatory feed was calculated with respect to the mean inlet concentration averaged over one period (1s). The lean inlet mixture is the most beneficial for CO and ethyne light-off, but deteriorates the conversion of NO. The stoichiometric feed is optimal as soon as conversions reach certain levels, what can be easily observed in the case of ethene. Oscillations can lead to a small conversion improvement at lower temperatures, when compared to the stoichiometric feed, but deteriorate the conversion after the light-off. The rich mixture leads to the slowest light-off and quite low conversions in all cases. Only the conversion of NO is somewhat higher, but also deteriorated with respect to the conversion when the stoichiometric feed is applied.

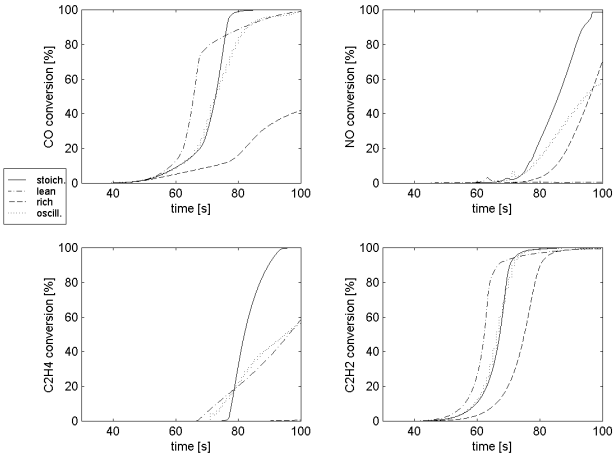

Figure 6. Conversions of reactants versus time after a linear increase in the feed temperature from 300K to 600K in 100s, with different input λ-s.

Secondary air injection – There are usually two reasons for introducing secondary air injection after the cold start: it increases the exhaust gas temperature, due to an exothermal reaction before the converter when the air is injected at the hot exhaust valve, and it provides the needed oxygen to the catalyst, if the engine runs rich, to prevent driveability problems [4]. The secondary air injection in this study is included in a simple way disregarding the exothermal reaction before the converter as well as the effect of exhaust gas cooling by the injected air. Dilution of the other components and higher space velocity have been taken into account. The oxygen (air) is added in the cases of a rich (λ=0.97) and a stoichiometric engine feed in such amounts that the converter input λ equals 1.15. Thus, in the case of rich engine feed more additional air has to be added. The inlet temperature again increases linearly from 300 to 600K in 100s. Fig. 7 shows CO conversion in both cases, with and without the additional injected air. It is clear that the additional oxygen in the inlet gas leads to a faster light-off of CO. It is in the line with the results shown in fig. 6. Although not shown, a similar result holds for ethyne. This faster light-off can be explained on the basis of chemical kinetics.

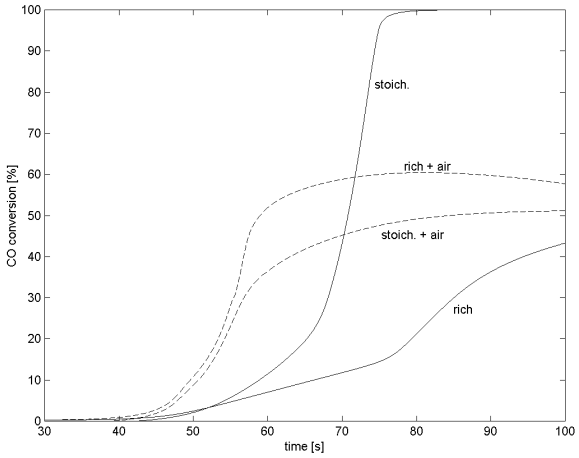

Figure 7. CO conversion versus time after a linear increase of the feed temperature from 300 to 600K in 100s, with and without the secondary air injection.

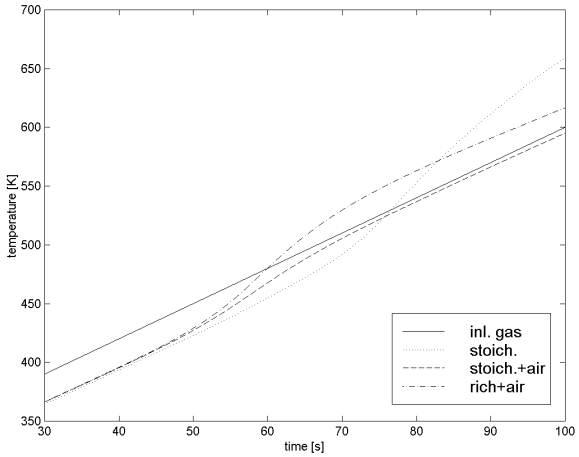

Figure 8. Solid temperature vs. time at 2.1cm from the reactor inlet for the same conditions as in fig. 7.

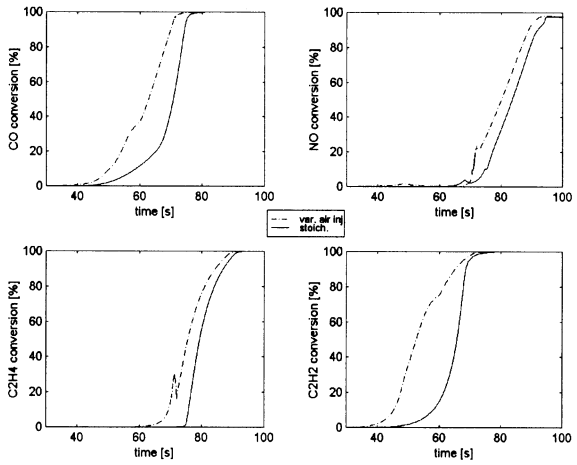

Figure 9. Conversion of components vs. time after the increase in the feed temperature from 300 to 600K in 100s, with and without the variable secondary air injection.

One of the problems at the low temperatures is that oxygen has difficulties to reach the surface because CO and ethyne have much higher adsorption rates. In that way the oxidation of CO and ethyne is actually inhibited by CO and ethyne themself. In the case of a rich mixture there is more CO and less oxygen in the exhaust gas, which retards the light-off even more. By introducing more oxygen via secondary air injection, more oxygen can reach the catalyst surface, because the adsorption rate is proportional to the solid phase concentration of oxygen. This leads to a faster oxidation of CO and ethyne. It also leads to a faster internal heating of the converter due to the released heat of reaction. During the warming-up of the reactor, reactions mostly occur in the warmer, front part of the reactor, so the reaction heat will mainly be released in the front part as well. Fig. 8 shows the solid temperature profile versus time at 2.1 cm from the reactor inlet in the cases of stoichiometric, stoichiometric + air and rich + air inlets. Note that all temperature differences result from different reaction heat release. This heat release can be related to the CO light-off shown in fig 7. It starts faster in the case of secondary air injection and is the highest with a rich engine mixture, because of higher CO and oxygen concentrations. After the reactions have been “ignited”, high inlet lambda resulting from secondary air injection is not favorable any more because the catalytic surface becomes extensively covered with oxygen. In this situation stoichiometric operation becomes optimal. Thus, when the reaction ignition occurs, the inlet lambda should be decreased back to the stoichiometry, see fig. 7. This may lead to an improvement in the conversion of all components. Fig. 9 shows the conversion vs. time for all four components compared to the stoichiometric conversion without the secondary air injection. The injected air starts being decreased at 60s, in such manner that the converter input λ decreases linearly from λ=1.15 at 60s to λ=1 at 72s. This way of operating the injected air can be beneficial since the light-offs of the various components occur in a sequence. After ethyne and CO have been oxidized, stoichiometric lambda improves the oxidation of ethene and the reduction of NO. The increased surface temperature also helps in that matter. The feature observed in NO and ethene conversion at 72s results from the increase in NO reduction as λ becomes stoichiometric which than leads to the decrease in ethene oxidation at that moment.

EXHAUST EMISSIONS CONTROL SYSTEM

In order to develop a reliable simulation model of the whole system that can later be used for control design, one has to take into account a relevant spark ignition engine dynamic behavior. A Mean Value Engine Model (MVEM) was selected, because it is rather simple and describes the most important engine variables on time scales somewhat larger than an engine cycle [27,28,29,30,31]. Such a model is very suitable for control purposes. Since the model used was basically adopted from the literature [28,30,31] it will not be described here in detail. The MVEM used here mainly describes the air-fuel mixture formation. Two main subsystems are the intake manifold and the fuel delivery. The intake manifold subsystem accounts for manifold air charging and a key equation is the manifold pressure state equation:

$$\frac{dp_m}{dt} = \frac{RT_m}{V_m}\left(\frac{dm_{at}}{dt} - \frac{dm_{ap}}{dt}\right) \tag{12}$$

This is a nonlinear state equation since the port air mass flow is a nonlinear function of manifold pressure and engine speed, while the throttle air mass flow is a nonlinear function of manifold pressure and throttle angle. The fuel delivery subsystem accounts for a wall fuel film formation in the manifold and/or port. This causes a fuel lag since the liquid fuel from the film can only enter the cylinder after evaporation or by slowly flowing toward the intake valve. This process is more important at low temperatures, where a larger fraction of fuel enters the film while it takes more time for fuel from the film to evaporate. A very simple, but often applied, fuel film model is:

$$\begin{aligned}\frac{dm_{ff}}{dt} &= X\frac{dm_{fi}}{dt} - \frac{m_{ff}}{\tau_e}\\ \frac{dm_{fc}}{dt} &= \frac{m_{ff}}{\tau_e} + (1-X)\frac{dm_{fi}}{dt}\end{aligned} \tag{13}$$

The parameters X and τ_e represent the amount of fuel entering the film and the evaporation time constant, respectively. Since the underlying process is quite complicated [32], these parameters are nonlinear functions of engine speed, manifold pressure and temperature. They are usually determined through identification [31,33], producing parameter maps for different engine operating conditions.

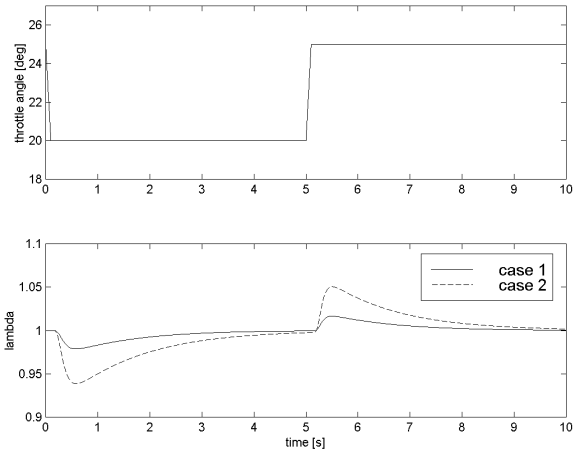

Figure 10. Engine model lambda responses on throttle changes with control model-process parameter mismatches of 10% (case 1) and 30% (case 2).

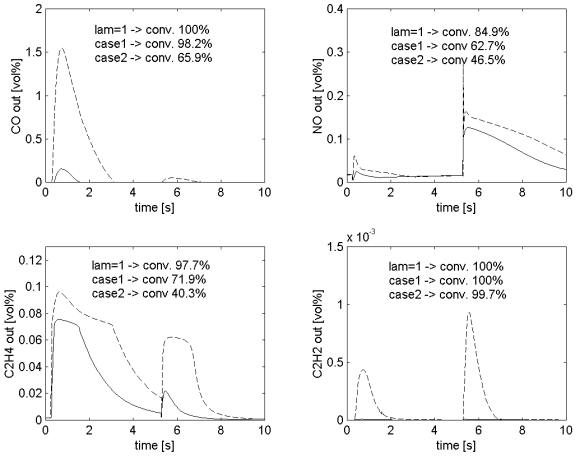

Figure 11. Responses of the converter outlet concentrations with the converter inlet temperature of 480K, in the cases given in fig. 10.

The given engine model, including also the relevant transport delays, was coupled with the catalytic converter model to simulate the complete system. Some simulation results are presented here. This model will be used for controller design. Fig. 10 presents the engine model lambda responses on the throttle ramp change from 25° to 20° and back. The air path is assumed to be perfectly modeled in the controller, thus the control algorithm "knows" exactly the amount of air induced into the cylinder per engine cycle. The amount of fuel injected is calculated on the basis of a feedforward control algorithm, which compensates for the wall wetting dynamics. Such compensation is common and was investigated by many authors, see eg. [31]. If the complete wall wetting dynamic behavior could be completely described by eq. (13), and if parameters X and τ_e would be exactly known, then such a control scheme would lead to an ideal λ control. Since this is almost never the case two situations with controller–process parameter mismatching were simulated together with the resulting effect on the catalytic converter. The nominal X and τ_e parameters are taken as 0.4 and 1s respectively and they are included into the control algorithm. The first case simulates a modeling error of 10% (X=0.44, τ_e=1.1s), while the second case simulates a modeling error of 30% (X=0.52, τ_e=1.3s). The effect of the model mismatching on the converter conversion is shown in fig. 11. The simulations were done with a converter inlet temperature of 480K. The conversion is calculated as an average over the given time period, assuming that the input concentrations remain the same as if λ=1. It is clear that lambda excursions mostly effect the NO and ethene conversion. These species are more difficult to be converted, so a small rich excursion deteriorates the ethene conversion, while lean excursion deteriorates the NO conversion. Ethyne is converted easily so its conversion does not deteriorate with these lambda excursions. Small lambda excursions (10% parameter mismatch) do not lead to lower CO conversion due to reaction with the oxygen stored on ceria. Large excursions (30% parameter mismatch), however, can not be compensated by the oxygen storage capacity and the CO conversion is reduced.

CONCLUSIONS

Catalyst converter behavior at low temperatures was investigated by development of a transient model based on elementary step kinetics. The converter light-off process can be understood through the competition of different species for the catalytic surface, leading to differences in a single-component and a multi-component light-off. A manipulation of the converter input lambda value only does not give a lot of freedom in the optimization of the light-off process. An important additional degree of freedom can be included through added oxygen via the secondary air injection. It allows more oxygen to reach the catalyst surface and to be available for the oxidation of ethyne and CO at lower temperatures. With some lambda manipulation it can then lead to faster light-off of all components. The main converter dynamic behavior to be considered in a control system comes from the oxygen storage on ceria. Rate constants related to that process determine the dynamic behavior of the whole converter.

The inclusion of an engine dynamic model completes the simulation model and leads to a good starting point for investigation of control strategies. The catalytic converter model will have to be reduced for that matter by keeping only the relevant dynamic behavior. It has been shown that a tight control is very important for converter performance. The future work will also include the validation of both engine and converter model, since they are currently based on literature data (different reactions were modeled on different catalysts) thus providing only the qualitative behavior of the system.

REFERENCES

1. Powell, J.D., Fekete, N.P. and Chang, C.F., "Observer-Based Air-Fuel Ratio Control", IEEE Cont. Sys. Mag., vol. 18, no.5, 72-83, 1998.
2. Guzzella, L., "Models and Modelbased Control of IC Engines – A Nonlinear Approach", SAE Technical Paper No. 950844, 1995.
3. Turin, R.C. and Geering, H.P., "Model-Based Adaptive Fuel Control in an SI Engine", SAE Technical Paper No. 940374, 1994.
4. Kollmann, K., et al., "Secondary Air Injection with a New Developed Electrical Blower for Reduced Exhaust Emissions", SAE Technical Paper No. 940472, 1994.
5. Katashiba, H., et al., "Development of an Effective Air-Injection System with Heated Air for LEV/ULEV", SAE Technical Paper No. 950411, 1995.
6. Oh, S.H., Bisset, E.J., Brown, D.B. and Ament, F., "Mathematical Modelling of Electrically Heated Monolith Converters: Power and Energy Reduction Strategies", SAE Technical Paper No. 961213, 1996.
7. Glander, D. and Zidat, S., "Mathematical Modeling of Electrically Heated Monolith Converters: Meeting European Emissions Regulations Proposed for 2000 and 2005", SAE Technical Paper No. 972852, 1997.
8. Silverston, P.L., "Automotive exhaust catalysis under periodic operation", Catal. Today 25, 175-195, 1995.
9. Taylor, K.C. and Sinkevitch, R.M., "Behavior of Automobile Exhaust Catalysts with Cycled Feedstreams", Ind. Eng. Chem. Prod. Res. Dev. 22, 45-51, 1983.
10. Tagliaferri, S., Koeppel, R.A. and Baiker, A., "Behavior of Non-Promoted and Ceria-Promoted Pt/Rh and Pd/Rh Three-Way Catalysts under Steady State and Dynamic Operation of Hybrid Vehicles", Ind. Eng. Chem. Res. 38, 108-117, 1999.
11. Oh, S.H. and Cavendish, J.C., "Transients of Monolithic Catalytic Converters: Response to Step Changes in Feedstream Temperature as Related to Controlling Automobile Emissions", Ind. Eng. Chem. Prod. Res. Dev. 21, 29-37, 1982.
12. Pattas K.N., et al., "Transient Modeling of 3-Way Catalytic Converters", SAE Technical Paper No. 940934, 1994.
13. Koltsakis, G.C., Konstantinidis, P.A. and Stamatelos, A.M., "Development and application range of mathematical models for 3-way catalytic converters", Appl. Catal. B: Environmental. 12, 161-191, 1997.
14. Montreuil C., Williams S. and Adamszyk A., "Modeling current generation catalytic converters: Laboratory experiments and kinetic parameter optimization – Steady state kinetics", SAE Technical Paper No. 920096, 1992.
15. Shafai, E., Roduner, C. and Geering, H.P., "Indirect Adaptive Control of a Three-Way Catalyst", SAE Technical Paper No. 961038, 1996.
16. Lie A.B.K., Hoebink, J.H.B.J. and Marin, G.B., "The Effects of Oscillatory Feeding of CO and O_2 on the Performance of a Monolithic Catalytic Converter of Automobile Exhaust Gas: A Modelling Study", Chem. Eng. J. 53, 47-54,1993.
17. Nievergeld, A.J.L., v. Selow, E.R., Hoebink, J.H.B.J. and Marin G.B., "Simulation of a catalytic converter of automotive exhaust gas under dynamic conditions", Stud. Surf. Sc. Catal. 109, 449-458, 1997.
18. Taylor, G.I., "Dispersion of soluble matter in solvent flowing through a tube", Proc. Roy. Soc. A219, 186, 1953.
19. v. Selow, E.R., "Design of a monolithic reactor for automobile exhaust gas conversion with improved light-off", Graduate Report, Institute for Continuing Education, Eindhoven University of Technology, 1996.
20. Impens, R., "Automotive Traffic: Risks for the Environment", Stud. Surf. Sc. Catal. 30, 11-30, 1987.
21. Mabilon, G., Durand, D. and Courty, Ph., "Inhibition of Post-Combustion Catalysts by Alkynes: A Clue for Understanding their Behaviour under Real Exhaust Conditions", Stud. Surf. Catal. 96, 775-788, 1995.
22. Hoebink, J.H.B.J., v. Gemert, R.A., v.d. Tillaart, J.A.A. and Marin, G.B., "Competing reactions in three-way catalytic converters: modelling of the NO_x conversion maximum in the light-off curves under net oxidising conditions", accepted for publication in Chem. Eng. Sc.
23. Oh, S.H., Fisher, G.B., Carpenter, J.E. and Goodman, D.W., "Comparative Kinetic Studies of CO-O_2 and CO-NO Reactions over Single Crystal and Supported Rhodium Catalysts, J. Catal. 100, 360-376, 1986.
24. Sant, R., Kaul, D.J. and Wolf, E.E., "Transient Studies and Kinetic Modeling of Ehylene Oxidation on Pt/SiO_2", AIChE J. 35(2), 267-278, 1989.
25. Nibbelke, R.H., Nievergeld, A.J.L., Hoebink, J.H.B.J. and Marin G.B., "Development of a Transient kinetic model for the CO Oxydation by O_2 over a Pt/Rh/CeO_2/g-Al_2O_3 three-way Catalyst", Appl. Catal. B: Environmental 19, 245-259, 1998.
26. NAG Fortran Library Manual, mark 15, vol. 1, 1991.
27. Aquino, C.F., "Transient A/F Characteristics of the 5 Liter Central Fuel Injection Engine", SAE Technical Paper No. 810494, 1981.
28. Hendricks, E. and Sorenson, S.C., "Mean Value Modeling of Spark Ignition Engines", SAE Technical Paper No. 900616, 1990.
29. Fiaschetti, J. and Narasimhamurthi, N., "A Descriptive Bibliography of SI Engine Modeling and Control", SAE Technical Paper No. 950986, 1995.
30. Hendricks, E., et al., "Modelling of the Intake Manifold Filling Dynamics", SAE Technical Paper No. 960037, 1996.
31. Almkvist, G. and Eriksson, S., "A Study of Air to Fuel Transient Response and Compensation with Different Fuels", SAE Technical Paper No. 941931, 1994.

32. Curtis, E.W. Aquino, C.F., Trumpy, D.K and Davis, G.C., “A New Port and Cylinder Wall Wetting Model to Predict Transient Air/Fuel Excursions in a Port Fuel Injected Engine”, SAE Technical Paper No. 961186, 1996.
33. Onder, C.H., Roduner, C.A. and Geering, H.P., “Model Identification for the A/F Path of an SI Engine”, SAE Technical Paper No. 970612, 1997.

NOTATION

a_{cat}: washcoat surface area
a_v: geometric surface area
A: pre-exponential factor
c_p: specific heat
C: concentration
d_b: monolith channel diameter
d_w: washcoat thickness
E_{act}: activation energy
k: rate coefficient
k_f: mass transfer coefficient
L_{NM}: noble metal capacity
L_{OSC}: oxygen storage capacity
m_{ap}: port air mass
m_{at}: throttle air mass
m_{fc}: fuel mass entering a cylinder
m_{ff}: fuel film mass
m_{fi}: injected fuel mass
M: molar mass
p: pressure
r: reaction rate
R: gas constant
s^o: sticking probability on clean surface
T: temperature
V: volume
X: fraction of injected fuel entering the film
α: heat transfer coefficient
$\Delta_r H$: reaction enthalpy
ε: monolith converter void fraction
ε_w: washcoat porosity
Φ_m^{sup}: superficial mass flow
θ: fractional surface coverage
λ: thermal conductivity
ρ: density
τ_e: evaporation time constant

SUBSCRIPTS:

a: adsorption
d: desorption
f: bulk gas phase
m: manifold
s: surface
w: washcoat